IEICE TRANSACTIONS

on Electronics

VOL. E104-C NO. 1
JANUARY 2021

A PUBLICATION OF THE ELECTRONICS SOCIETY

The Institute of Electronics, Information and Communication Engineers
Kikai-Shinko-Kaikan Bldg., 5-8, Shibakoen 3 chome, Minato-ku, TOKYO, 105-0011 JAPAN

IEICE TRANS. ELECTRON., VOL.E104–C, NO.1 JANUARY 2021

PAPER

Effect of Tunnel Pits Radius Variation on the Electric Characteristics of Aluminum Electrolytic Capacitor

Daisaku MUKAIYAMA[†,††a)], ***Nonmember and*** **Masayoshi YAMAMOTO**[††], ***Member***

SUMMARY Aluminum Electrolytic Capacitors are widely used as the smoothing capacitors in power converter circuits. Recently, there are a lot of studies to detect the residual life of the smoothing Aluminum Electrolytic Capacitors from the information of the operational circuit, such as the ripple voltage and the ripple current of the smoothing capacitor. To develop this kind of technology, more precise impedance models of Aluminum Electrolytic Capacitors become desired. In the case of the low-temperature operation of the power converters, e.g., photovoltaic inverters, the impedance of the smoothing Aluminum Electrolytic Capacitor is the key to avoid the switching element failure due to the switching surge. In this paper, we introduce the impedance calculation model of Aluminum Electrolytic Capacitors, which provides accurate impedance values in wide temperature and frequency ranges.

key words: *aluminum electrolytic capacitor, tunnel pit, impedance*

1. Introduction

The electric characteristics of Aluminum Electrolytic Capacitors had been analyzed by using the transmission line model, which was introduced by R. H. Broadbent to calculate the impedance of the anode foil pits. On the other hand, R. M. Peekema and J. P. Beesley used the transmission line model to calculate the impedance of Foil-type Electrolytic Capacitors [1], [2]. After that, a lot of impedance models of Aluminum Electrolytic Capacitors have been proposed based on this transmission line model [3], [4]. If the anode foil pits are regarded as cylindrical holes, then, the pit impedance is estimated by Eq. (3). The pit impedance depends on the pit geometry, in particular, radius and length. However, the variations of the pit configurations, such as the pit length or the pit radius, have been unconsidered. The length of tunnel pits is manufactured to have the same length as possible to keep the foil strength as shown in Fig. 1 (a). Therefore, we neglect the pit length and consider the effect of the tunnel pit radius variation on the impedance of Aluminum Electrolytic Capacitors in this paper. We reveal that the pit radius of etched foils follows not a normal distribution, but a log-normal distribution, as shown in Fig. 1 (b). Figure 1 (b) is concerned with the etched foil 115HD9 before anodization, and which data was provided by JCC (Japan Capacitor Industrial Co., Ltd.) of this etched foil

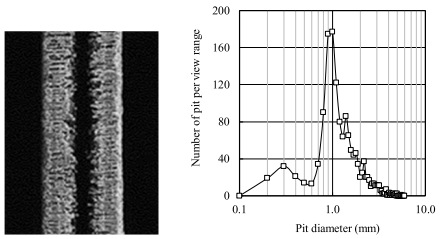

Fig. 1 (a) The typical anode foil etching pattern SEM images. (b) The pit diameter distribution of DC etched foil before anodization (provided by JCC).

manufacture. In the following discussion, the effect of the pit radius distribution on the impedance of Aluminum Electrolytic Capacitors is evaluated from the results of the Monte-Carlo simulations. Furthermore, we discuss the resistance of paper and electrolyte system which is expected to be enlarged by the high current density near the pit opening. Lastly, a new complex relative permittivity ε_r expression of the anodized film based on the response function is applied to this calculation [5]. This paper shows that the impedance of Aluminum Electrolytic Capacitors can be well-represented for wide temperature and frequency ranges by taking into account these three items, (i) the tunnel pit radius deviation, (ii) the effect of the tunnel pit opening to the resistance of spacer paper and electrolyte system, (iii) the dielectric description based on the response function.

2. Theory and Models

2.1 The Impedance Model of the Anode Foil with Tunnel Pits

We proceed with the discussion about the impedance model of Aluminum Electrolytic Capacitors whose anode foils have tunnel patterns (cylindrical pits) as shown in Fig. 1 (a). In the pit configuration, we assume that the lengths of pits are constant value l_p and the distribution of the pit radius follows the log-normal distribution. The first target is to calculate the impedance of the basic structure per one pit with the density in the number of pits N_{pit}. Figure 2 (a) explains the concept of the basic structure. The pit radius is defined as r_{pit}, the average pit radius is r_{pit_mu}, and the standard deviation of the pit radius is σ_{pit}. The complete list of symbols is given in Sect. 7 Nomenclature in this paper. The pit impedance Z_{pit} is composed of the dielectric (capacitance) part on the sidewall of the tunnel and the electrolyte

Manuscript received February 28, 2020.
Manuscript revised June 1, 2020.
Manuscript publicized July 14, 2020.
[†]The author is with Rubycon Corporation, Ina-shi, 399–4593 Japan.
[††]The authors are with Power Electronics Laboratory, Nagoya University, Nagoya-shi, 464–8601 Japan.
a) E-mail: mukaiyamad@rubycon.co.jp
DOI: 10.1587/transele.2020ECP5009

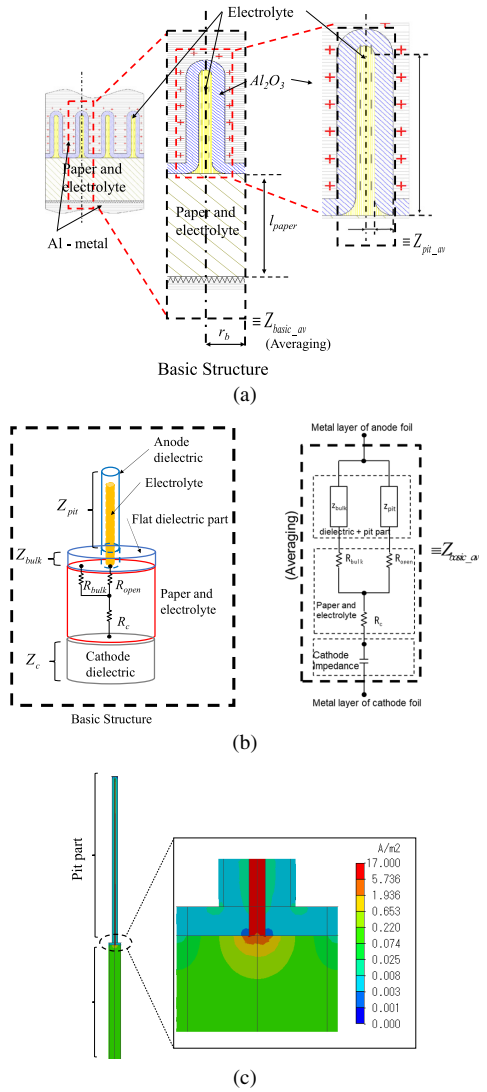

Fig. 2 (a) The basic structure, (b) the equivalent circuit of the basic structure, (c) The FEM simulation result of the current density in the basic structure

(resistance) part fulfilling the tunnel as in Fig. 2, and it is calculated by the transmission-line model fwhich includes the distributed capacitance of the dielectric and distributed resistance of the electrolyte. The pit capacitance: C_{pit} and the electrolyte resistance: R_{pit} from the pit opening to the pit end are given by Eqs. (1) (2) respectively. Thus, the impedance of the tunnel pit is given by Eq. (3) referring to Broadbent's work [1]. This equation ignores the component of the flat end of pits. The impedance of the flat end is too small, so it is neglectable.

$$C_{pit} = \varepsilon_r \varepsilon_0 \frac{2\pi l_{pit}}{\ln(1 + d/r_{pit})} \tag{1}$$

$$R_{pit} = \frac{\rho_{ele} l_{pit}}{\pi {r_{pit}}^2} \tag{2}$$

$$Z_{pit} = \sqrt{\frac{R_{pit}}{j\omega C_{pit}}} \coth \sqrt{j\omega R_{pit} C_{pit}}$$

$$= e^{-j\frac{\pi}{4}} \sqrt{\frac{\rho_{el} \ln(1+d/r_{pit})}{2\pi^2 \omega \varepsilon_0 \varepsilon_r {r_{pit}}^2}} \coth\left[e^{j\frac{\pi}{4}} \left(\frac{l_{pit}}{r_{pit}} \right) \sqrt{\frac{2\omega\varepsilon_0\varepsilon_r\rho_{el}}{\ln(1+d/r_{pit})}} \right] \tag{3}$$

Where j represents the imaginary unit, and the complex relative permittivity of the dielectric ε_r and the electrolyte resistivity ρ_{el} are provided with complex numbers. The complex relative permittivity ε_r is given below [5].

$$\varepsilon_r(\omega) = \varepsilon_r'(\omega) - j\varepsilon_r''(\omega) \tag{4}$$

$$\varepsilon_r'(\omega) = \varepsilon_{r\infty} + \varepsilon_{r0}(\tau_{di}\omega)^{-(1-n)}\Gamma(2-n)\cos\{(1-n)\pi/2\} \tag{5}$$

$$\varepsilon_r''(\omega) = \varepsilon_{r0}(\tau_{di}\omega)^{-(1-n)}\Gamma(2-n)\sin\{(1-n)\pi/2\} \tag{6}$$

$$1 - n(T) = \beta T \tag{7}$$

$$\tau_{di}(T) = \tau_{di0}\exp[u/T] \tag{8}$$

Seeing Eq. (3), we find that the significant parameters to the pit impedance Z_{pit} are the ratio of the dielectric thickness d to the pit radius r_{pit} and the ratio of the pit length to the pit radius. Therefore, the deviation of the pit radius should have a significant role in the Aluminum Electrolytic Capacitor impedance especially for the high-frequency and low-temperature range. Because the electrolyte resistivity ρ_{el} exponentially increases as temperature decreasing. To calculate the averaging pit impedance based on the pit distribution which follows a log-normal distribution, we introduce Monte-Carlo method to make the pit radius series as shown in Appendix A. The parameters to give the log-normal distribution are (i) the average value r_{pit_mu} and (ii) the standard deviation σ_{pit}. After getting a large number of the pit radius which follows the above log-normal distribution, the averaging pit impedance Z_{pit_av} can be obtained by applying them to Eq. (3). If the density in the number of pits N_{pit} is known, the radius of the basic structure r_b in Fig. 2 (a) can be given by Eq. (9) without any geometric contradictions.

$$\pi {r_b}^2 = 1/N_{pit} - \pi\left\{(r_{pit\_mu}+d)^2 + {\sigma_{pit}}^2\right\} + \pi(r_{pit}+d)^2 \tag{9}$$

The relation Eq. (9) is used to derive Eq. (10), and it holds on a log-normal distribution.

$$\left\langle (r_{pit}+d)^2 \right\rangle = (r_{pit\_mu}+d)^2 + {\sigma_{pit}}^2 \tag{10}$$

Where the bracket $< >$ denotes to take averaging under the log-normal distribution. By using Eq. (9), the impedance of the flat dielectric part in the anode foil of the basic structure is given by

$$Z_{bulk} = -j\omega\varepsilon_0\varepsilon_r \Big/ d\left[1/N_{pit} - \pi\left\{(r_{pit\_mu}+d)^2 + {\sigma_{pit}}^2\right\}\right]. \tag{11}$$

Therefore, the anode foil impedance per unit macroscopic area is estimated by

$$z_{anode} = N_{pit}(Z_{pit\_av} + Z_{bulk}). \tag{12}$$

Thus, the problem is how to determine the density in the number of pits N_{pit}. Generally, the specification of the foil

used for Aluminum Electrolytic Capacitors defines the measurement method of the capacitance per unit area. The specifications of the foil contain the details of the measurement method, such as the ingredients and the formation of the measurement electrolyte, the resistivity of the measurement electrolyte, and the temperature and the frequency of the measurement. Therefore, we can determine N_{pit} so that the specified capacitance of the anode foil is equal to the capacitance derived by Eq. (12). On carrying out the determination of N_{pit} based on the calculation of Eq. (12), the values of the electrolyte resistivity, frequency and temperature are given by the same values of the anode foil specification or the anode foil capacitance measurement condition.

2.2 Introduction of "Basic structure" and Its Impedance Calculation

Once the density in the number of pits N_{pit} is determined, the radius of the basic structure r_b in Fig. 2 (a) is given by Eq. (9). The next step is to calculate the impedance of the electrolyte and spacer paper system of the basic structure. As explained in the introduction, the narrow pit opening has an impact on the resistance of the electrolyte and spacer paper system. As shown in Fig. 2 (c), the current density near the pit opening is large, and the current density on the flat dielectric is small. On the other hand, the current density on the cathode surface becomes a constant value. These situations mean that the resistance enlargement effect by the narrow pit opening occurs near the underneath of the pit opening and that this effect does not appear in the part which is far from the anode foil surface. Therefore, the equivalent circuit of the paper and electrolyte system of the basic structure may be represented by three resistances: R_{bulk}, R_{open}, and R_c as shown in Fig. 2 (b). These resistances should satisfy the below simultaneous equations,

$$\begin{cases} R_{open} + R_c = f_{open} R_{ep} \\ R_{bulk} + R_c = f_{bulk} R_{ep} \\ R_{open} \,//\, R_{bulk} + R_c = R_{ep} \end{cases}. \tag{13}$$

Where the symbol of the double slash is defined as the parallel connection of two impedance as below,

$$A \,//\, B \equiv \frac{AB}{A+B}. \tag{14}$$

R_{ep} is the resistance between the top surface and the bottom surface of the cylinder of the paper and electrolyte system, and it is given by

$$R_{ep} = \frac{\rho_{es} d_p}{\pi {r_b}^2}. \tag{15}$$

$f_{open} R_{ep}$ corresponds to the resistance from the pit opening to the bottom surface, and $f_{bulk} R_{ep}$ is to the resistance from the surface of the flat anode dielectric to the bottom surface. According to Appendix B, the factors f_{pit} and f_{bulk} are given by

$$f_{open} = \left(\frac{r_{pit}}{r_b}\right)^2 + 2\sum_{n=1}^{\infty} \frac{1}{(J_2(x_{1n}))^2} \cdot \frac{J_1(x_{1n} r_{pit}/r_b)}{x_{1n} r_{pit}/r_b} \left(\frac{\tanh(x_{1n} d_p/r_b)}{x_{1n} d_p/r_b} - 1 \right), \tag{16}$$

$$f_{bulk} = \frac{2}{1-(r_{pit}/r_b)^2} \sum_{n=1}^{\infty} \left[\frac{1}{(J_2(x_{1n}))^2} \cdot \frac{J_1(x_{1n} r_{pit}/r_b)}{x_{1n} r_{pit}/r_b} \left(\frac{\tanh(x_{1n} d_p/r_b)}{x_{1n} d_p/r_b} J_0(x_{1n}) - 1 \right) \right]. \tag{17}$$

The complex resistivity of the electrolyte and spacer paper system can be calculated as below,

$$\rho_{es} = \frac{1}{1/(\kappa_s \rho_{el}) + j\varepsilon_0 \varepsilon_{r\_es} \omega}. \tag{18}$$

Here, we assume that the permittivity of the electrolyte and spacer paper system is given by the parallel connection of the paper fiber and the electrolyte which fills the paper void, then, the permittivity of the electrolyte and spacer paper system becomes

$$\varepsilon_{r\_es} = (1-p)\varepsilon_{r\_paper} + p\varepsilon_{r\_el}. \tag{19}$$

The simultaneous equations (13) are easily solved and the below equations are obtained.

$$R_{open} = a_{open} R_{ep}, \tag{20}$$

$$R_{bulk} = a_{bulk} R_{ep}, \tag{21}$$

$$R_c = a_c R_{ep}. \tag{22}$$

Where,

$$a_{open} = (f_{open} - 1) + \sqrt{(f_{open}-1)(f_{bulk}-1)}, \tag{23}$$

$$a_{bulk} = (f_{bulk} - 1) + \sqrt{(f_{open}-1)(f_{bulk}-1)}, \tag{24}$$

$$a_c = 1 - \sqrt{(f_{open}-1)(f_{bulk}-1)}. \tag{25}$$

The cathode surface impedance per one basic structure is simply given by

$$Z_c = \frac{1}{\pi {r_b}^2} \left(-j\frac{1}{c_c \omega} + \frac{\tan\delta_c}{c_c \omega} \right). \tag{26}$$

These aforementioned equations give the impedance per one basic structure as below,

$$Z_{basic} = (Z_{pit} + R_{open}) \,//\, (Z_{bulk} + R_{bulk}) + R_c + Z_c. \tag{27}$$

By taking the average of the above impedance of the basic structure with the Monte-Carlo calculation of r_{pit}, the averaging impedance of the basic structure is obtained, and the impedance per macroscopic area between the anode metal layer and the cathode metal layer is given by

$$z_p = \langle Z_{basic} \rangle / N_{pit}. \tag{28}$$

Where, the bracket means taking the average by the Monte-Carlo numerical calculation that the pit radius distribution follows the log-normal distribution (average value: r_{pit_mu}, standard deviation: σ_{pit}).

2.3 The Capacitor Impedance

The capacitor impedance can be derived by the same method proposed in Ref. [2], which considers the capacitor circuit as the strip-line. The shunt impedance is calculated by Ohm's law, that is,

$$Z_{shunt\_1} = z_p / W l_1. \tag{29}$$

The series impedance from the lead tab to the edge of the anode foil is given by Ohm's law with considering the skin-effect for high frequency as below,

$$Z_{series\_1} = \frac{l_1}{W}\left(\frac{\rho_{effect}(\theta,\omega,t_a)}{t_a} + \frac{\rho_{effect}(\theta,\omega,t_c)}{t_c}\right). \tag{30}$$

With,

$$\rho_{effect}(\theta,\omega,t) = \rho_{Al}(\theta)\frac{x}{2}\frac{1+e^{-x}}{(1-e^{-x})^2}, \tag{31}$$

$$x = t/\delta_{skin}, \tag{32}$$

$$\delta_{skin} = \sqrt{\frac{2\rho_{Al}(\theta)}{\mu_0\omega}}, \tag{33}$$

$$\rho_{Al}(\theta) = \rho_{Al}(20^\circ C)\{1 + \alpha_{Al}(\theta - 20)\}. \tag{34}$$

Then, the capacitor impedance of one part (divided in two-parts at the lead tab location) is given by

$$Z_1 = \sqrt{Z_{series\_1} Z_{shunt\_1}}\coth\sqrt{\frac{Z_{series\_1}}{Z_{shunt\_1}}}. \tag{35}$$

The impedance of the other part Z_2 (from the lead tab to another anode foil edge) is given by the below equations.

$$Z_{shunt\_2} = z_p / W l_2, \tag{36}$$

$$Z_{series\_2} = \frac{l_2}{W}\left(\frac{\rho_{effect}(\theta,\omega,t_a)}{t_a} + \frac{\rho_{effect}(\theta,\omega,t_c)}{t_c}\right), \tag{37}$$

$$Z_2 = \sqrt{Z_{series\_2} Z_{shunt\_2}}\coth\sqrt{\frac{Z_{series\_2}}{Z_{shunt\_2}}}. \tag{38}$$

The parasitic inductance exists due to the current path which is formed from the outer anode terminal to the cathode terminal. This parasitic inductance is represented by L_{para}. Furthermore, the two lead tabs (cathode and anode) resistance should be significant in a high-frequency range. The two lead tabs resistance is obtained in the same way as Eq. (30) as below,

$$R_{tabs} = 2 \times \frac{l_{tab}}{W_{tab}}\frac{\rho_{effet}(\theta,\omega,t_{tab})}{t_{tab}}. \tag{39}$$

Then, finally, the capacitor impedance is given by

$$Z_{cap} = Z_1 \,//\, Z_2 + jL_{para}\omega + R_{tabs}. \tag{40}$$

3. Experimental

The specifications of the capacitors under test are as follows: "400V / 280μF / D25mm X L40mm". These capacitors were fabricated with the following raw materials.

Table 1 The parameters used for the calculation.

Parameter	Values	unit	Parameter	Values	unit
d	0.580	µm	l_{pit}	43	µm
c_a	0.318	µF/cm^2	t_a	29.8	µm
ε_{r0}	9.85	-	$\varepsilon_{r\infty}$	1.00	-
β	2.169 $\times 10^{-5}$	-	τ_{di0}	2.837 $\times 10^{-16}$	sec.
u	2886	°K	c_c	195	µF/cm^2
$tan\delta_c$	0.01	-	t_c	28.8	µm
κ_s	19.4	-	d_p	30	µm
ε_{r_paper}	7.0	-	p	0.503	-
ε_{r_el}	40	-	α_{Al}	4.2×10^{-3}	-
$\rho_{Al}(20°C)$	2.75 $\times 10^{-8}$	Ω·m	W	31	mm
l_1	690	mm	l_2	790	mm
W_{tab}	4	mm	l_{tab}	50	mm
t_{tab}	200	µm	L_{para}	12	nH

Anode foil: 120HB15S-580V (HEC), Cathode foil: 50CK (JCC), Spacer Paper: PE4-30 (NKK), Electrolyte: resistivity 600Ωcm at 30°C (an organic acid ammonium salt in a solvent mainly containing ethylene glycol). The anode lead tab is cold-welded with the anode foil at 690mm from the edge of the anode foil as listed in Table 1. The cathode lead tab cold-welded points are located close to the anode cold-welding points. The Impedance frequency characteristics were measured by the precision LCR meter, E4980A (Agilent Technology) in the Low-temperature chamber, MC-811T (ESPEC).

The measurement by the LCR meter was made with a-c Max. 0.5Vrms of sinusoidal voltage without d-c bias. The cables connecting the LCR meter to the test capacitors were coaxial cables with 50Ωcm characteristic impedance by the four-terminal pair method. The measured frequency and temperature were as below.

- Frequency: 20Hz, 60Hz, 100Hz, 120Hz, 200Hz, 300Hz, 360Hz, 500Hz, 1kHz, 2kHz, 5kHz, 10kHz, 20kHz, 50kHz, 100kHz, 200kHz, 500kHz, 1MHz.
- Temperature: −40°C, −25°C, −10°C, 0°C, 20°C, 25°C, 40°C, 60°C, 85°C, 105°C.

The viscosity of the electrolyte used for the capacitors under test was measured in the temperature range: −40°C~125°C to compare the interpolated resistivity function, which was derived from the resistivity data measured by the general conductivity meter (cell type). The viscosity was measured by the viscometer SVM TM 3001 (Anton Paar). The complex conductivity of the electrolyte at 25°C was measured in the frequency range: 3kHz~9GHz by the Vector Network Analyzer, ZVL (ROHDE&SHWARZ).

4. Results

Figure 3 (a) shows the plot of the electrolyte resistivity values which are calculated by the interpolate function (41) versus the measurement viscosity data in the temperature range: −40°C~125°C. The linearity can be found in a low-temperature range. That means Eq. (41) should be correct even for the low-temperature range.

$$\rho_{el}(\theta) = 30.07\exp[-2.114\times10^{-6}\theta^3$$

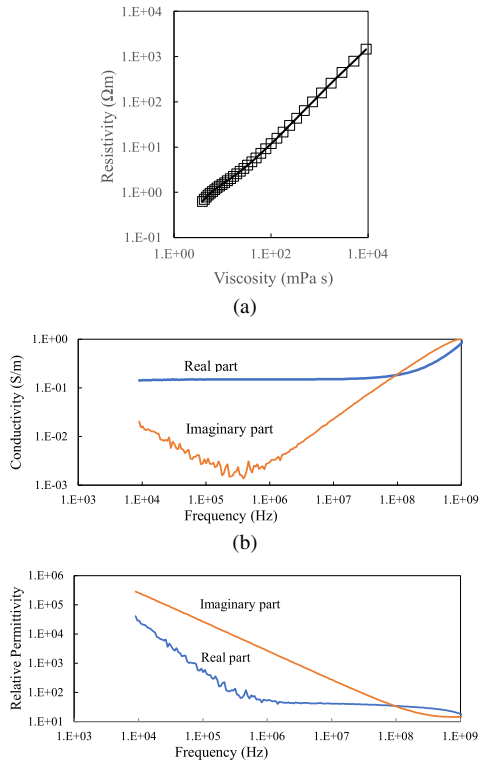

Fig. 3 The operational electrolyte characteristics.

$$+ 5.789 \times 10^{-4}\theta^2 - 7.032 \times 10^{-2}\theta] \quad (\Omega\text{m}) \tag{41}$$

Figure 3 (b) and Fig. 3 (c) show the complex conductivity and the relative permittivity of the electrolyte respectively at 25°C. The imaginary part of the conductivity below 200kHz is increasing due to the electric double-layer capacitance on the electrode. Therefore, the electrolyte conductivity and the real part of the permittivity should be considered as constant values below 10MHz. The electrolyte dielectric dispersion appears above 10MHz since the real part of the permittivity is decreasing. From these measurements of the electrolyte used for the capacitors under test, Eq. (41) should be accurate in the temperature range: −40°C∼105°C and in the frequency below 10MHz. As to the relative permittivity of the electrolyte, it is reasonable to consider the real part value as a constant value equals 40, and the imaginary part can be negligible below 10MHz.

The metal layer thickness values of the anode foil and the cathode foil were derived by the measurement of the resistance concerning the foil length. The estimated metal layer thickness of the anode foil t_a and the cathode foil t_c are listed in Table 1. The pit length in the listing column l_{pit} was derived as half of the value subtracting the metal layer thickness from the anode foil thickness (116μm). The parameters of the anode foil dielectric are referred to as the articles published by us for the same capacitors under test [5]. The surface impedance parameters of the cathode foil are given in Table 1. The thickness of the dielectric film, aluminum oxide layer, is 0.58μm since the forming voltage of the anode foil is 580V (EIAJ) and the dielectric thickness is about 0.1nm / 1V for the oxidization in a conventional boric acid solution. The parameters of spacer paper shown in Table 1 were derived with the cellulose density: 1.5(g/cm^3) and the data shown in the manufacturer datasheet (NKK). And we set the permittivity of the paper fiber as the cellulose value: 7.0. The other dimensions in Table 1 are obtained by measuring the raw materials of the capacitor under test.

Table 2 The density in the number of pits

r_{pit_mu} (μm)	σ_{pit} (μm)	N_{pit} (pcs/m^2)	*Note.*
0.455	0.405	1.219×10^{11}	Refer to Fig.4 and Fig. 7(a).
0.370	0.000	1.372×10^{11}	Refer to Fig. 6(a).
0.350	0.100	1.426×10^{11}	Refer to Fig. 6(b) and Fig. 7(b).

We carried out Monte Carlo calculation with the number of samples: 10^6, thus the calculation result will have three significant figures. Table 2 shows the example calculation results of the pit density N_{pit} for each pit radius distribution condition derived by Eq. (12) with the anode foil capacitance $0.97c_a$. The factor of 0.97 will be explained later.

Figure 4 (a) shows that the capacitance calculations precisely reproduced in overall frequency and temperature ranges. The absolute values of impedance and ESR are shown in Fig. 4 (c) and Fig. 4 (d) respectively. The calculation values of impedance and ESR tend to be lower than the experimental values in a high-frequency side in the range below −10 °C. Figure 4 (b) shows the log-log plot of the relative capacitance to the value of 20Hz and 105°C versus the frequency. As comparing Fig. 4 (c) (d) with Fig. 4 (b), the impedance and ESR values tend to deviate from the experimental values over the frequency on which the relative capacitance begins to deviate. These deviations appear above the frequency where the relative capacitance is 0.01. The reason for this deviation will be discussed in the following section.

There are two points that we adjusted on the numerical calculation shown in Fig. 4. The first point is that the electrolyte resistivity is multiplied by the factor: 0.85. Because the winding element of the Aluminum Electrolytic Capacitor has the residual moisture, the true electrolyte resistivity in the capacitor is difficult to be obtained. The second point is that the capacitance reproduction ratio of the test capacitors. We use the factor 0.97 by which multiplies the anode foil capacitance c_a to derive the number of density of pits. Because the capacitance per area is reduced in the operational electrolyte of the real capacitor compared to in the electrolyte for the foil capacitance measurement, and the complex permittivity ε_r of the anode dielectric has been derived by the capacitance data of the test sample capacitors [5]. The clear evidence of how to determine these two factors currently does not exist. But these values are generally used for the Aluminum Electrolytic Capacitor design process.

Based on the above parameters and the two adjusting

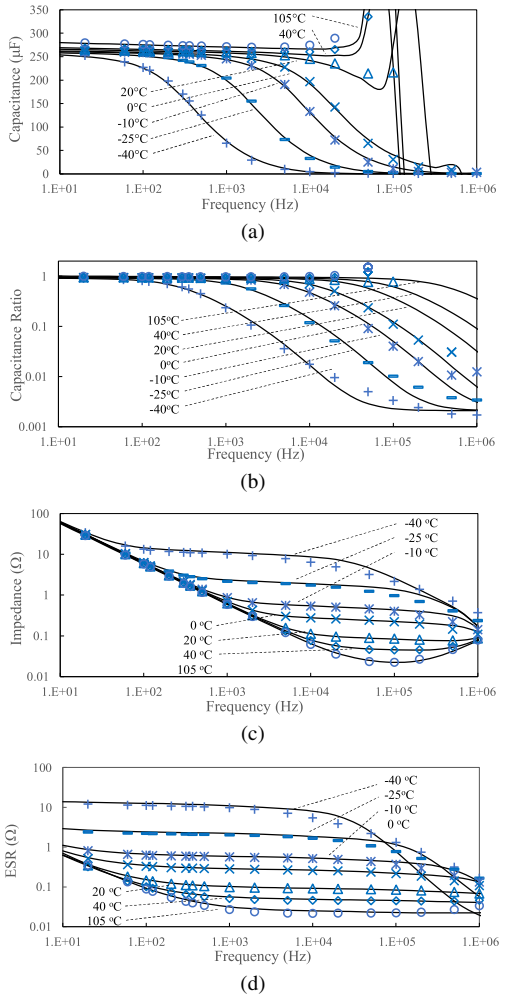

Fig. 4 The comparison of the measurement data with the calculation results. The solid lines correspond to the calculation under r_{pit_mu} = 0.455μm, σ_{pit} = 0.405μm, and the Marks are to the measurements.

factors, we optimized the pit distribution parameters for the measured capacitance data at −40°C. Because the capacitance variation with a change in frequency due to the pit geometry becomes more obvious at a lower temperature. We define the objective function: *Error* of optimization as the sum of the square of the deviation between the calculation value and the measurement data. The frequency range of the data used for the optimize calculation is taken from 20Hz to 10kHz since the measured capacitance data above 10kHz contains the parasitic inductance component.

$$Error = \sum_{i=1(20Hz)}^{12(10kHz)} (C_{meas}(-40^{\circ}C, f_i) - C_{cal}(-40^{\circ}C, f_i))^2 \tag{42}$$

Where, $C_{meas}(-40^{\circ}C, f_i)$ is the measurement capacitance value at f_i (Hz) and −40°C, $C_{cal}(-40^{\circ}C, f_i)$ is the calculation capacitance under the same condition, and f_i (Hz) is the measuring frequency series as explained in Sect. 3. The 3D plot of the objective function magnitude versus r_{pit_mu} and σ_{pit} is shown in Fig. 5. The values: r_{pit_mu} = 0.455μm and

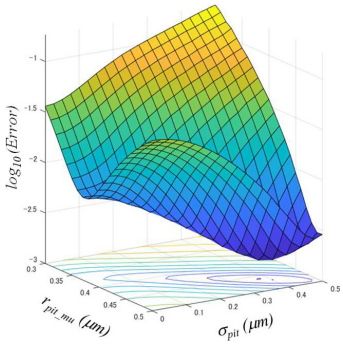

Fig. 5 The error function of the calculation to the measurement capacitance data at −40C.

σ_{pit} = 0.405μm are obtained as the optimization point.

5. Discussion

As shown in Fig. 4, the calculated impedance values are consistent with the measurement data. The model calculation results can reproduce the capacitance characteristics and the dissipation by the anode foil dielectric. That implies that the dielectric theory based on the response function of Eq. (43) can represent the dielectric properties of the oxidized film of Aluminum Electrolytic Capacitors [5].

$$\varphi(t) = \frac{1-n}{\tau_{di}}\left(\frac{t}{\tau_{di}}\right)^{-n} \tag{43}$$

The deviation from the measurement data becomes remarkable in the high frequency at −25°C and −40°C. The density in the number of pits is estimated to be 1.219×10^{11} pcs/m^2 for the present anode foil parameters in Table 1. Then, the capacitance ratio of the flat dielectric part to the pit part is deduced to be 0.03. Figure 4 (b) shows the capacitance ratio to the value at 20Hz and 105°C versus frequencies. The deviation of the capacitance ratio between the measurement and the calculation becomes remarkable above the frequency where the capacitance ratio is reaching to 0.03. That is, the present model gives a good agreement in the range where the anode foil capacitance appears in the impedance characteristics. Thus, it concludes, that the reason for the deviation between the calculated values and the measurement values is that the impedance calculation of the electrolyte and paper system in a low-temperature range is not accurate. It had been reported that the paper dispersion should have significant effects on the impedance of the Aluminum Electrolytic Capacitors at low-temperature, and the colloidal dispersion of the electrolyte and spacer paper system should be related to this deviation [6].

To see the effect of the variation in the pit diameter, we calculate the capacitance for the model whose pit diameters are uniform without any variation. Taking the same way as the calculation of Fig. 4, we optimize the average pit diameter r_{pit_mu} to minimize the object error function. The optimized value of r_{pit_mu} is estimated to be 0.35μm for the no variance distribution as shown in Fig. 5, and the capacitance

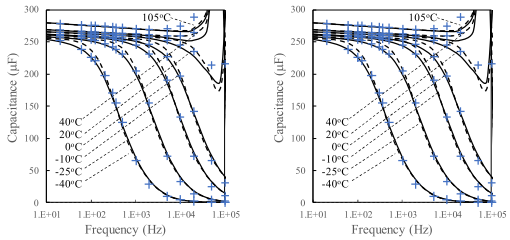

Fig. 6 (i) The solid line corresponds to r_{pit_mu} = 0.455μm, σ_{pit} = 0.405μm, (ii) Mark "+" is to the measurement data. (iii) the broken line in (a) is to r_{pit_mu} = 0.37μm and σ_{pit} = 0μm, and (iv) the broken line in (b) is to r_{pit_mu} = 0.35μm and σ_{pit} = 0.1μm.

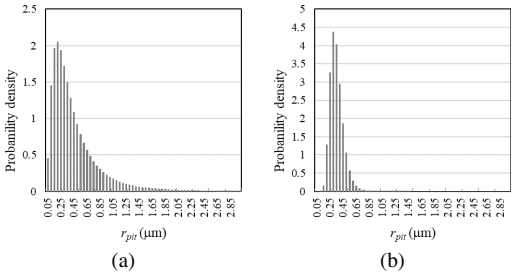

Fig. 7 The probability density of the pit diameter. (a) corresponds to r_{pit_mu} = 0.455μm, σ_{pit} = 0.405μm, the maximum frequency value is 0.19μm. (b) corresponds to r_{pit_mu} = 0.35μm, σ_{pit} = 0.1μm, the maximum frequency value is 0.31μm.

calculation results are shown in Fig. 6 (a). Comparing these results, the deviation of no variance distribution model from the measurement becomes large in a low-frequency range, where the capacitance remains more than 150μF. Thus, it follows that the variation of the pit radius should be a significant element to describe the impedance characteristics, in the range where the capacitance reduction ratio is within about 50%.

To evaluate the resistance enlargement effect on the electrolyte and spacer paper system by narrow pit openings, we conduct the calculation without this effect. That is, it corresponds that the parameters of Eqs. (20)~(22) are set as a_{open} = a_{bulk} = 0 and a_c = 1. Same as the above calculations, we take the optimization of the pit radius distribution and obtain the values r_{pit_mu} = 0.35μm, σ_{pit} = 0.1μm for it. The results are shown in Fig. 6 (b), where we compare these results with the calculation results in Fig. 4 (a) and measuring data. As previously explained, the deviation, in the range where the capacitance reductions remain within 50%, mainly comes from the geometric effect of pits. The capacitance reduction in a high-frequency range becomes less compared to the measurement data or the calculation results of Fig. 4 (a) due to neglecting this effect.

Figure 8 shows the pit radius distributions. One is the histogram which follows the parameters r_{pit_mu} = 0.455μm, σ_{pit} = 0.405μm, the other follows the parameter r_{pit_mu} = 0.35μm, σ_{pit} = 0.1μm. The most frequent values in radius for these two distributions are deduced 0.19μm for the former and 0.31μm for the latter. Figure 8 shows the SEM

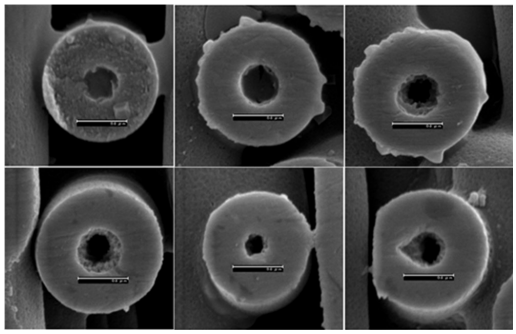

Fig. 8 The SEM images of the cross-section of the tunnel pit provided by Rubycon Corporation. The bar's length indicates 0.6μm. The specimens are sampled from the same anode foil, 120HD10-665Vf (JCC).

images of the pit part cross-section of the anode foil replica. This sampled foil of Fig. 8 is different from what is used for the capacitors under test. However, the pit radius will not be so different from that of the impedance measurement capacitors. From these SEM images, the pit radius distribution will be more likely to be the former distribution than the latter one.

6. Conclusion

The presented modeling method of the Aluminum Electrolytic Capacitors gives a precise reproduction of the impedance values for a wide range of temperature and frequency because this method is considering three elements. (i) The dielectric dispersion of the anode foil based on the response function, (ii) the statistic information of the pit radius, (iii) the enhanced factor to the resistance of the electrolyte and spacer paper system due to current concentration under the pit opening. In the present impedance calculation, the two uncertain factors were need. One is the electrolyte resistivity correction factor due to absorbing the remaining moisture. The other is the factor regarding the dielectric constant to compensate between the anode foil capacitance measured in the specified electrolyte and the capacitance in the operational electrolyte. The former factor can be deduced by researching the remaining moisture amount of the capacitor element before impregnating the electrolyte. The latter seems to be difficult to calculate theoretically. Because the interfacial dielectric phenomena between the electrolyte and the Aluminum Oxide surface should be related to this capacitance reduction factor [6].

The present calculation results show good agreement with the measuring impedance data within the range that the capacitance remains 3% of the static capacitance. The ratio of 3% corresponds to the capacitance of the flat dielectric part of the anode foil. Therefore, the remaining problem to make more precise models is how to describe the capacitance reduction phenomena of this 3% amount of capacitance. As well as the above capacitance compensation in the operational electrolyte, this phenomenon will be related to the interfacial dielectric between the electrolyte and the Aluminum Oxide surface.

7. Nomenclature

ω: Angular frequency.
T: Absolute Temperature.
θ: Temperature in Celsius degree.
ε_0: Space permittivity.
μ_0: Space permeability.
d: Thickness of the aluminum oxide layer (dielectric).
r_{pit}: The pit radius.
r_{pit_mu}: The average pit radius.
σ_{pit}: The standard deviation of pit radius.
l_{pit}: The length of the pits
N_{pit}: The density in the number of pits.
r_b: The radius of the basic structure.
t_a: The thickness of the anode foil metal layer.
t_c: The thickness of the cathode foil metal layer.
W: The width of anode foil (Cathode foil).
l_1: The length of anode foil from the lead tab to the foil edge.
l_2: The length of anode foil from the lead tab to the other edge.
ε_r: Complex permittivity of the Aluminum oxide (dielectric).
ε'_r: The real part of εr.
ε_r'': The imaginary part of εr.
ε_{r0}: The electric relative permittivity for the static limit.
$\varepsilon_{r\infty}$: The electric relative permittivity for the infinity frequency.
$\tau_{di}(T)$: The Relaxation time of the Aluminum oxide (dielectric) at T (°K).
τ_{di0}: The Relaxation time at 0 (°K).
1-n: The power index of ω term of the response function.
u: The activation energy (°K) of the relaxation time.
c_a: The capacitance per area of the anode foil by specified measurement.
c_c: The capacitance per area of the cathode foil.
$tan\,\delta_c$: The dissipation factor of the cathode foil.
ρ_{el}: The resistivity of electrolyte.
ε_{r_el}: The relative permittivity of the electrolyte.
ε_{r_paper}: The relative permittivity of the spacer paper.
κ_s: The enlargement factor of the electric resistivity by the spacer paper.
p: The porosity of the spacer paper
d_p: The thickness of the spacer paper.
ρ_{es}: The complex resistivity of the electrolyte and spacer paper system.
ε_{r_es}: The relative permittivity of the electrolyte and spacer paper system.
ρ_{efect}: The effective resistivity with considering the skin-effect.
ρ_{Al}: The direct current resistivity of Aluminum.
α_{Al}: The temperature coefficient of the Aluminum resistivity.
l_{tab}: The length of the lead tab.
W_{tab}: The width of the lead tab.
t_{tab}: The thickness of the lead tab.
R_{tabs}: The resistance of the lead tabs.
Z_{pit}: The impedance of one pit part (Dielectric + electrolyte).
Z_{pit_av}: The averaged value of Z_{pit} by Monte-Carlo calculation.
Z_{bulk}: The impedance of the flat (bulk) part in the basic structure.
z_{anode}: The anode foil impedance per macroscopic area (the averaged value by Monte-Carlo calculation).
Z_c: The impedance of the cathode foil in the basic structure.
z_p: The basic structure impedance per macroscopic area (the averaged value by Monte-Carlo calculation.)
R_{ep}: The resistance of the electrolyte and spacer paper system calculated by the Ohm law.
R_{open}: The resistance of the electrolyte and spacer paper system near the pit opening.
R_{bulk}: The resistance of the electrolyte and spacer paper system near the flat dielectric part of the anode foil.
R_c: The resistance of the electrolyte and spacer paper system far from the anode foil.
Z_{shunt_1}: The shunt impedance of one part (divided into two parts at the lead tabs).
Z_{shunt_2}: The shunt impedance of the other part.
Z_{seires_1}: The series impedance of one part (divided into two parts at the lead tabs).
Z_{seires_2}: The series impedance of the other part.
Z_1: The impedance of one part (divided into two parts at the lead tab).
Z_2: The impedance of the other part.
L_{para}: The parasitic inductance of the capacitor.
Z_{cap}: The capacitor impedance.

Acknowledgments

The author wishes to express his thanks to Dr. Mostafa for English proofreading, to Dr. T. Yamaguchi in Nagoya University for measuring the permittivity of electrolyte and to Mr. S. Hoshino in Rubycon Corporation for providing SEM images of anode foils.

References

[1] R.H. Broadbent, "Aluminum Foil Electrolytic Capacitors," Electrochemical Technology, vol.6, no.5-6, pp.163–166, May-June 1968.
[2] R.M. Peekema and J.P. Beesley, "Factors Affecting the Impedance of Foil-Type Electrolytic Capacitors," Electrochemical Technology, vol.6, no.5-6, pp.166–172, May-June 1968.
[3] A.R. Morley, "Effect of Electrolyte Resistance in Porous Anodes," Proc. IEEE, vol.117, no.8, pp.1648–1654, Aug. 1970.
[4] S.G. Parler, "Improved Spice Models of Aluminum Electrolytic Capacitors for Inverter Applications," IEEE Trans. Ind. Appl., vol.39, no.4, pp.929–935, July/Aug. 2003.
[5] D. Mukaiyama and M. Yamamoto, "Dielectric Characteristics Analysis of Aluminum Electrolytic Capacitors Based on Linear Response Function," J. Electrochem. Soc., vol.166, no.16, pp.E554–E563, 2019.
[6] R.S. Alwitt, "Contribution of Spacer Paper to the Frequency and temperature Characteristics of Electrolytic Capacitors," J. Electrochem. Soc., vol.116, no.7, pp.1024–1027, July 1969.
[7] http://pmsl.planet.sci.kobe-u.ac.jp/~seto/?page_id=316&lang=ja, Feb. 25th, 2020.
[8] G.E.P. Box and M.E. Muller, "A Note on the Generation of Ran-

dom Normal deviates," Ann. Math. Statist., vol.29, no.2, pp.610–611, 1958.

Appendix A: Generation of Random Log-Normal Deviates [7]

Supposed the log-normal distribution for the variant x with the average value m and the standard deviation s, the distribution of $\log x$ should follow the normal distribution. Here, the average value and the standard deviation of the $\log x$ distribution are denoted by μ and σ respectively, and the variable X is defined by

$$X = \log x. \tag{A·1}$$

The variable X follows the normal distribution with the average μ and the standard deviation σ. Then,

$$\begin{aligned}&\frac{1}{\sqrt{2\pi}\sigma}\exp\left[-\frac{(X-\mu)^2}{2\sigma^2}\right]dX\\ &=\frac{1}{\sqrt{2\pi}\sigma x}\exp\left[-\frac{(\log x-\mu)^2}{2\sigma^2}\right]dx.\end{aligned} \tag{A·2}$$

Thus, the log-normal distribution function $f(x)$ is given by

$$f(x)=\frac{1}{\sqrt{2\pi}\sigma x}\exp\left[-(\log x-\mu)/2\sigma^2\right]. \tag{A·3}$$

Here, the domain of variable x becomes $(0,\infty)$. The average value of x under the distribution (A·3) is obtained as below,

$$\begin{aligned}m&=\int_0^\infty xf(x)dx\\ &=\frac{1}{\sqrt{2\pi}\sigma}\int_0^\infty dx\exp\left[-(\log x-\mu)^2/2\sigma^2\right].\end{aligned} \tag{A·4}$$

We replace the variable x to X and change the variable domain $(0,+\infty)\rightarrow(-\infty,+\infty)$. Then, Eq. (A·4) is calculated as below.

$$\begin{aligned}m&=\frac{1}{\sqrt{2\pi}\sigma}\int_{-\infty}^\infty\exp\left[-(X-\mu)^2/2\sigma^2\right]e^X dX\\ &=\frac{1}{\sqrt{2\pi}\sigma}\int_{-\infty}^\infty\exp\left[-\frac{1}{2\sigma^2}\left\{X-(\mu+\sigma^2)\right\}^2+\mu+\frac{1}{2}\sigma^2\right]dX\\ &=\exp\left[\mu+\sigma^2/2\right]\end{aligned} \tag{A·5}$$

The variance s^2 is given by

$$s^2=\int_0^\infty dx(x-m)^2f(x)=\int_0^\infty dxx^2f(x)-m^2. \tag{A·6}$$

Therefore, the variance s^2 is obtained from the expectation value of x^2, which is denoted by $<x^2>$. Then, $<x^2>$ is calculated as below,

$$\begin{aligned}\left\langle x^2\right\rangle&=\int_0^\infty x^2f(x)dx\\ &=\frac{1}{\sqrt{2\pi}\sigma}\int_0^\infty x\exp\left[-(\log x-\mu)/2\sigma^2\right]dx.\end{aligned} \tag{A·7}$$

By the same relation between the variance and the average of Eq. (A·5) for Eq. (A·7), the following result is obtained,

$$\left\langle x^2\right\rangle=e^{2(\mu+\sigma^2)}. \tag{A·8}$$

Taking the square of Eq. (A·5), then,

$$m^2=e^{2\mu+\sigma^2}. \tag{A·9}$$

Therefore,

$$\left\langle x^2\right\rangle=e^{2(\mu+\sigma^2)}=m^2e^{\sigma^2}. \tag{A·10}$$

The relation of Eq. (A·10) is applied to Eq. (A·6), then, the variance s^2 is given by

$$s^2=m^2\left(e^{\sigma^2}-1\right). \tag{A·11}$$

Thus,

$$s=m\sqrt{e^{\sigma^2}-1} \tag{A·12}$$

From Eq. (A·9) and Eq. (A·11), μ and σ are expressed by m and s as below,

$$\mu=\log m-\frac{1}{2}\log\left(1+s^2/m^2\right), \tag{A·13}$$

$$\sigma=\sqrt{\log(1+s^2/m^2)}. \tag{A·14}$$

Therefore, if we give the average value m and the standard deviation s of the log-normal distribution, the corresponding average μ and standard deviation σ of the normal distribution are obtained by Eq. (A·13) and Eq. (A·14) respectively. Here, the random number series following the log-normal distribution is denoted by x_i, and the random number following the normalized normal distribution ($\mu=0$, $\sigma=1$) is presented by $Rn(0,1)$. Then,

$$x_i=\exp[\sigma\,Rn(0,1)+\mu]. \tag{A·15}$$

The random number $Rn(0,1)$ can be obtained by the general mathematical methods. In this paper, the Box-Muller method [8] is used, and it has the below formula,

$$\begin{cases}z_1=(-2\log u_1)^{1/2}\cos 2\pi u_2\\ z_2=(-2\log u_1)^{1/2}\sin 2\pi u_2\end{cases}. \tag{A·16}$$

Where, u_1 and u_2 are the independent random number in $[0,1]$ domain. The values z_1 and z_2 are to be distributed as following the normalized normal distribution ($\mu=0$, $\sigma=1$).

Appendix B: The Impedance Calculation of the Paper and Electrolyte Part of the Basic Structure

We consider the cylinder as shown in Fig. A·1 with the electric resistivity: ρ, the radius: a and the height: h. The electric potential of the bottom surface is set to be zero, and the normal component of the electric field on the cylindrical surface is set to be zero. The disk-like electrode with the radius: b is disposed of the center of the top surface of the cylinder,

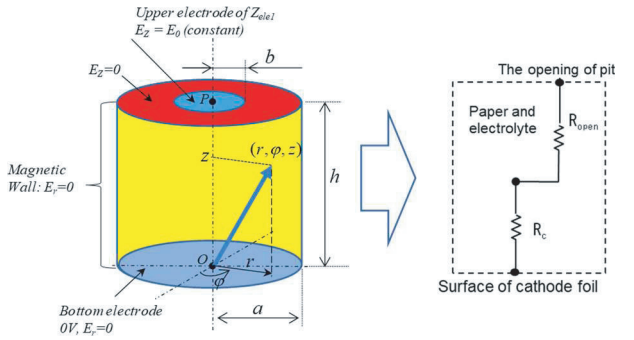

Fig. A·1 The Model of the electrolyte and spacer paper system in the basic structure. In Appendix B, a, b and h correspond to r_{pit}, r_b, and d_p respectively, the value of $R_{open} + R_c$ is to the impedance Z_{ele1}, and the value of $R_{bulk} + R_c$ in Fig. 2 (b) is to Z_{ele2}.

where the electric field E_1 is a constant vector with the vertical direction. The vertical component of the electric field is set to be zero at the top surface of the cylinder except for the disk-like electrode $(b \le r \le a)$. Then, the impedance between the bottom of the cylinder and the disk-like electrode on the top is to be estimated as the following. We supposed the electric potential ϕ as the below separable function with introducing cylindrical coordinates. Then,

$$\phi(r, \varphi, z) = R(r)\Phi(\varphi)Z(z). \tag{B·1}$$

Since the potential has symmetry about the center axis, the potential becomes the function of r and z as below,

$$\phi(r, z) = R(r)Z(z). \tag{B·2}$$

We consider now the boundary conditions. The bottom of the cylinder is set to be zero in the electric potential, that is,

$$\phi(0 \le r \le a, 0) = 0. \tag{B·3}$$

Since the electric field of the upper electrode is the constant vector normal to the surface and directed inward, the boundary condition on the upper electrode is given by

$$-\left(\frac{\partial \phi}{\partial z}\right)_{0 \le r \le b, z=h} = -E_1. \tag{B·4}$$

The top surface of the cylinder except the upper electrode is set to be a magnetic wall. Then,

$$\left(\frac{\partial \phi}{\partial z}\right)_{b \le r \le a, z=h} = 0. \tag{B·5}$$

The boundary conditions of Eq. (B·4) and Eq. (B·5) can be written by the step function θ as below,

$$-\left(\frac{\partial \phi}{\partial z}\right)_{z=h} = -E_1 \theta(b - r). \tag{B·6}$$

Since the electric field must be symmetry to the cylindrical surface of the basic structure, the current should flow into the vertical (z) direction there. Thus, the magnetic wall boundary should be applied to the cylindrical surface of the basic structure. That is,

$$\left(\frac{\partial \phi}{\partial r}\right)_{r=a} = 0. \tag{B·7}$$

The calculation area has no charge, and both the permittivity and the conductivity are constant. Thus, the potential of the cylinder follows the below Laplace equation,

$$\nabla^2 \phi(r, z) = 0. \tag{B·8}$$

That is,

$$\frac{1}{r}\frac{\partial}{\partial r}\left(r\frac{\partial \phi}{\partial r}\right) + \frac{\partial^2 \phi}{\partial z^2} = 0. \tag{B·9}$$

Substituting Eq. (B·2) into Eq. (B·9) and dividing by $R \cdot Z$, then,

$$\frac{1}{R}\left[\frac{1}{r}\frac{\partial}{\partial r}\left(r\frac{\partial R}{\partial r}\right)\right] + \frac{1}{Z}\frac{\partial^2 Z}{\partial z^2} = 0. \tag{B·10}$$

The first term of the left-hand side is the function of r and the second term is the function of z. Thus, these two terms should be a constant value. Therefore, Eq. (B·10) should satisfy the below equations,

$$\frac{1}{R}\left[\frac{1}{r}\frac{\partial}{\partial r}\left(r\frac{\partial R}{\partial r}\right)\right] + \kappa^2 = 0; \tag{B·11}$$

$$\frac{\partial^2 Z}{\partial z^2} = \kappa^2 Z. \tag{B·12}$$

Furthermore, such a solution of oscillating in the z-ffdirection is neglectable, that is,

$$\kappa^2 \ge 0. \tag{B·13}$$

In the case of $\kappa = 0$, the solution is composed of $R = C_{r1} log r + C_{r2}$ and $Z = C_{z1} z + C_{z2}$. As the potential should not diverge at $r = 0$, thus, $C_{r1} = 0$, and R must be constant values. From the boundary condition of Eq. (B·3), the potential is equal to zero at $z = 0$. Therefore, $C_{r2} = 0$, and $C_{z2} = 0$. The general solution of Eq. (B·12) is given by

$$Z(z) = A_z \cosh \kappa z + B_z \sinh \kappa z \quad \text{for } \kappa \ne 0; \tag{B·14}$$

$$Z(z) = C_z z \quad \text{for } \kappa = 0. \tag{B·15}$$

The boundary condition (B·3) requires $A_z = 0$. Here, the undetermined constants are represented by A_κ and C, the above equations are written by Eq. (B·16). Furthermore, in the case of $\kappa = 0$, the Eqs. (B·14) and (B·15) can be expressed by one equation from $sinh\, \kappa z = 0$. Thus,

$$Z(z) = A_\kappa \sinh \kappa z + C\delta_\kappa z. \tag{B·16}$$

Where, the suffix κ is added to the coefficient of $sinh\, \kappa z$ because it depends on the value of κ, and the Kronecker δ_κ is to the coefficient of z since it has a value only if $\kappa = 0$. Considering Eq. (B·11), Eq. (B·11) is straightforwardly calculated as below,

$$\frac{d^2 R}{dr^2} + \frac{1}{r}\frac{dR}{dr} + \kappa^2 R = 0. \tag{B·17}$$

Divided the above equation by r^2 and replaced by $\rho \equiv \kappa r$,

then,

$$\frac{d^2R}{d\rho^2} + \frac{1}{\rho}\frac{dR}{d\rho} + R = 0. \tag{B· 18}$$

Equation (B· 18) is the Bessel differential equation in the order 1st. To avoid the divergence at $r = 0$, the solution of Eq. (B· 18) should be given by

$$R(r) = A_r J_0(\kappa r). \tag{B· 19}$$

Where J_0 is the 0^{th} Bessel function in order 1^{st}. We substitute the Eqs. (B· 16) and (B· 19) into Eq. (B· 2). With considering the superposition, then,

$$\phi(r, z) = \sum_{\kappa}(A_\kappa \sinh \kappa z \cdot J_0(\kappa r) + \delta_\kappa C z). \tag{B· 20}$$

The coefficients, A_κ and C, are determined to satisfy the boundary conditions: (B· 4)~(B· 7). Applied the boundary condition (B· 7) to Eq. (B· 20), the following equation is required in the range: $0 \le z \le h$.

$$\left(\frac{\partial \phi}{\partial r}\right)_{r=a} = \sum_{\kappa} A_\kappa \sinh(\kappa z)\left(\frac{dJ_0(\kappa r)}{dr}\right)_{r=a} = 0. \tag{B· 21}$$

Thus, the parameter κ should satisfy,

$$\left(\frac{dJ_0(\kappa r)}{dr}\right)_{r=a} = 0. \tag{B· 22}$$

As the Bessel function $J_0(\rho)$ has the below relation with the Bessel function $J_1(\rho)$,

$$\frac{dJ_0(\rho)}{d\rho} = J_{-1}(\rho) = -J_1(\rho), \tag{B· 23}$$

so that the parameter κ should satisfy the following equation,

$$\kappa\left(\frac{dJ_0(\rho)}{d\rho}\right)_{r=a} = 0 \rightarrow J_1(\kappa a) = 0. \tag{B· 24}$$

Therefore, the values of κa are on the zero points of $J_1(\rho)$. Here, we represent the zero points of $J_1(\rho)$ by x_{1n} assigned by natural numbers n from the minimum zero-point. Here, the suffix *1* means the 1st Bessel function. Then, the required condition (B· 24) becomes

$$\kappa a = x_{1n}. \tag{B· 25}$$

We assign the allowed values of κ by n. Then, the following expression is obtained,

$$\kappa_n = x_{1n}/a. \tag{B· 26}$$

Therefore, the suffix κ of summation of Eq. (B· 20) can be replaced by n, then,

$$\phi(r, z) = \sum_{n=1} A_n \sinh \kappa_n z \cdot J_0(\kappa_n r) + Cz. \tag{B· 27}$$

The constant parameter A_n is determined by the boundary conditions (B· 4) and (B· 6). To proceed with it, we take the partial differential of Eq. (B· 27) in the direction z on the plane of $z = h$.

$$\left(\frac{\partial \phi}{\partial z}\right)_{z=h} = \sum_{n=1}^{\infty} A_n \kappa_n \cosh \kappa_n h J_0(\kappa_n r) + C. \tag{B· 28}$$

Applied the boundary condition (B· 6) to Eq. (B· 28), then,

$$\sum_{n=1} A_n \kappa_n \cosh \kappa_n h J_0(\kappa_n r) + C = E_1 \theta(b - r). \tag{B· 29}$$

Furthermore, we take the differential of Eq. (B· 29) and use the relation of Eq. (B· 23). Then, Eq. (B· 29) becomes

$$-\sum_{n=1} A_n {\kappa_n}^2 \cosh(\kappa_n h) J_1(\kappa_n r) = -E_1 \delta(r - b). \tag{B· 30}$$

Where $\delta(r - b)$ is the Dirac Delta function. As Eq. (B· 30) is regarded as the equation of the Delta function expanding series, we can derive the equation that the factor A_n should satisfy. For this purpose, we apply the Fourier-Bessel expansion to the delta function $\delta(r - b)$ in Eq. (B· 30) within the interval $0 \le r \le a$. Then, the below expression is obtained,

$$\delta(r - b) = 2\left(\frac{b}{a^2}\right)\sum_{n=1}^{\infty} \frac{J_1(\kappa_n b) J_1(\kappa_n r)}{(J_2(x_{1n}))^2}. \tag{B· 31}$$

Thus, Eq. (B· 31) becomes

$$\sum_{n=1} A_n {\kappa_n}^2 \cosh(\kappa_n h) J_1(\kappa_n r) = 2E_1\left(\frac{b}{a^2}\right)\sum_{n=1}^{\infty} \frac{J_1(\kappa_n b) J_1(\kappa_n r)}{(J_2(x_{1n}))^2}. \tag{B· 32}$$

Therefore, A_n is given by

$$A_n = \frac{2b}{\cosh(x_{1n} h/a)} \frac{J_1(x_{1n} b/a)}{{x_{1n}}^2 (J_2(x_{1n}))^2} E_1 \tag{B· 33}$$

In the derivation of Eq. (B· 33), we replace κ_n to x_{1n} with Eq. (B· 26). Substituting Eq. (B· 33) in Eq. (B· 27), then, the potential is given by

$$\phi(r, z) = 2bE_1 \sum_{n=1}^{\infty}\left[\frac{\sinh(x_{1n} z/a)}{\cosh(x_{1n} h/a)} \times \frac{J_1(x_{1n} b/a)}{{x_{1n}}^2 (J_2(x_{1n}))^2} J_0(x_{1n} r/a)\right] + Cz. \tag{B· 34}$$

The partial differential of (B· 34) in the direction of z at $z = h$ is

$$\left(\frac{\partial \phi}{\partial z}\right)_{z=h} = \left[2\frac{b}{a}\sum_{n=1}^{\infty} \frac{J_1(x_{1n} b/a)}{x_{1n}(J_2(x_{1n}))^2} J_0(x_{1n} r/a)\right] E_1 + C. \tag{B· 35}$$

The boundary condition (B· 6) is applied to Eq. (B· 35). Then,

$$E_1 \theta(b - r) = \left[2\frac{b}{a}\sum_{n=1}^{\infty} \frac{J_1(x_{1n} b/a)}{x_{1n}(J_2(x_{1n}))^2} J_0(x_{1n} r/a)\right] E_1 + C. \tag{B· 36}$$

Thus, the coefficient C is derived by the calculation of Eq. (B· 36) at $r = 0$ as below,

$$C = \left[1 - \frac{2b}{a}\sum_{n=1}^{\infty}\frac{J_1(x_{1n}b/a)}{x_{1n}(J_2(x_{1n}))^2}\right]E_1. \quad (\text{B}\cdot 37)$$

As the coefficients A_n and C are determined, we obtain the potential as below,

$$\phi(r,z) = \left[1 + 2\left(\frac{b}{a}\right)^2\sum_{n=1}^{\infty}\frac{1}{(J_2(x_{1n}))^2}\frac{J_1(x_{1n}b/a)}{x_{1n}b/a} \times\left\{\frac{\sinh(x_{1n}z/a)}{(x_{1n}z/a)\cosh(x_{1n}h/a)}J_0(x_{1n}r/a) - 1\right\}\right]zE_1. \quad (\text{B}\cdot 38)$$

We take the partial derivative of the potential (B· 38) with respect to z. Then, the z component of the electric field is obtained,

$$-\frac{\partial\phi}{\partial z} = -E_1\left[1 + \frac{2b}{a}\sum_{n=1}^{\infty}\frac{J_1(x_{1n}b/a)}{x_{1n}(J_2(x_{1n}))^2} \times\left\{\frac{\cosh(x_{1n}z/a)}{\cosh(x_{1n}h/a)}J_0(x_{1n}r/a) - 1\right\}\right]. \quad (\text{B}\cdot 39)$$

To estimate the impedance, we calculate the potential at ($r = 0$, $z = h$) by Eq. (B· 38). Then,

$$\phi(0,h) = \left[1 + 2\left(\frac{b}{a}\right)^2\sum_{n=1}^{\infty}\frac{1}{(J_2(x_{1n}))^2} \times\frac{J_1(x_{1n}b/a)}{x_{1n}b/a}\left\{\frac{\tanh(x_{1n}h/a)}{x_{1n}h/a} - 1\right\}\right]hE_1. \quad (\text{B}\cdot 40)$$

The z component of the electric field at ($r = 0$, $z = h$) is obtained by Eq. (B· 39), then,

$$\left(\frac{\partial\phi}{\partial z}\right)_{z=h} = E_1\left[1+\frac{2b}{a}\sum_{n=1}^{\infty}\frac{J_1(x_{1n}b/a)}{x_{1n}(J_2(x_{1n}))^2}(J_0(x_{1n}r/a)-1)\right]. \quad (\text{B}\cdot 41)$$

As the current density j is given by E_1/ρ according to the Ohm's law, and the area of the top electrode is πb^2, the input current I from the top electrode becomes

$$I = \left(\pi b^2/\rho\right)E_1. \quad (\text{B}\cdot 42)$$

Strictly, the potential at $z = h$ should be taken for the averaging value from $r = 0$ to $r = b$. However, the potential difference between $r = 0$ and $r = b$ is quite small because the Aluminum Electrolytic Capacitors hold the relation: $h \gg a$. Therefore, the impedance Z_{ele1} from the top electrode to the bottom is given by dividing Eq. (B· 40) with Eq. (B· 42), then,

$$Z_{ele1} = \frac{\rho h}{\pi b^2}\left[1 + 2\left(\frac{b}{a}\right)^2\sum_{n=1}^{\infty}\frac{1}{(J_2(x_{1n}))^2} \times\frac{J_1(x_{1n}b/a)}{x_{1n}b/a}\left(\frac{\tanh(x_{1n}h/a)}{x_{1n}h/a} - 1\right)\right]. \quad (\text{B}\cdot 43)$$

When the top electrode is given by the disk with the hole contrariwise, the electrode range becomes $b \le r \le a$. Then, the impedance Z_{ele2} from the top electrode to the bottom is derived in the same way and the result is as below,

$$Z_{ele2} = \frac{\rho h}{\pi a^2}\left[\left(\frac{b}{a}\right)^2 + 2\sum_{n=1}^{\infty}\frac{1}{(J_2(x_{1n}))^2} \times\frac{J_1(x_{1n}b/a)}{x_{1n}b/a}\left(\frac{\tanh(x_{1n}h/a)}{x_{1n}h/a} - 1\right)\right]. \quad (\text{B}\cdot 44)$$

Daisaku Mukaiyama received the B.S. and M.S. degrees in Physics from Science University of Tokyo, Chiba, in 1994 and 1996, respectively. From 1996, he was with Tokyo Measuring Instrument Lab, Tokyo, Japan. Since 1997, he has been with Rubycon Corporation and is currently purchasing the Ph.D. degree in Power Electronics Laboratory, Department Electrical Engineering in Nagoya University, Nagoya, Japan. His research interests include the modeling (thermal and electrical) of any type of capacitors.

T Masayoshi Yamamoto (M'11) received the M.S. and Ph.D. degrees in science and engineering from Yamaguchi University, Yamaguchi, Japan in 2000 and 2004, respectively. From 2004, he was with Sanken Electric Co., Ltd., Saitama, Japan. Since 2006, he has been with Shimane University, Matue, Japan. His research interests include power supplies for HEV (boost converter, buck-converter, three-phase inverter, digital control), charging systems for EVs, LED illumination systems for tunnels, EMI of switching power supplies, and wireless power transfer.